Global analysis of the stream power law parameters based on worldwide 10Be denudation rates

Global analysis of the stream power law parameters based on worldwide ^{10}Be denudation rates

M.-A. Harel*, S. M. Mudd, M. Attal

University of Edinburgh, School of GeoSciences, Drummond street, EH8 9XP Edinburgh, Scotland, UK

** Corresponding author: E-mail: mharel@staffmail.ed.ac.uk*

Abstract

The stream power law, expressed as $E = KA^mS^n$ — where E is erosion rate [LT^{-1}], K is an erodibility coefficient [T^{-1}L$^{(1-2m)}$], A is drainage area [L^2], S is channel gradient [L/L], and m and n are constants — is the most widely used model for bedrock channel incision. Despite its simplicity and limitations, the model has proved useful for topographic evolution, knick-point migration, palaeotopography reconstruction, and the determination of rock uplift patterns and rates. However, the unknown parameters K, m, and n are often fixed arbitrarily or are based on assumptions about the physics of the erosion processes that are not always valid, which considerably limits the use and interpretation of the model. In this study, we compile a unique global data set of published basin-averaged erosion rates that use detrital cosmogenic ^{10}Be. These data (N = 1457) enable values for fundamental river properties to be empirically constrained, often for the first time, such as the concavity of the river profile (m/n ratio or concavity index), the link between channel slope and erosion rate (slope exponent n), and substrate erodibility (K). These three parameters are calculated for 59 geographic areas using

the integral method of channel profile analysis and allow for a global scale analysis in terms of climatic, tectonic, and environmental settings. In order to compare multiple sites, we also normalise n and K using a reference concavity index $m/n = 0.5$. A multiple regression analysis demonstrates that intuitive or previously demonstrated local-scale trends, such as the correlation between K and precipitation rates, do not appear at a global scale. Our results suggest that the slope exponent is generally > 1, meaning that the relationship between erosion rate and the channel gradient is nonlinear and thus support the hypothesis that incision is a threshold controlled process. This result questions the validity of many regional interpretations of climate and/or tectonics where the unity of n is routinely assumed.

Keywords: stream power law; cosmogenic nuclide; denudation rates; climate; tectonics; lithology

---

1. Introduction

At geological timescales, river networks record the balance between constructive (tectonics) and destructive forces (mostly climate, via erosion) shaping landscapes (Fig. 1). This is why the study of fluvial incision is one of the cornerstones of geomorphology, providing insight into the processes (past and present) that modify landforms. During the last two decades, substantial progress has been made thanks to developments in the digital representation of topography (Fielding et al., 1994) and the measurement of denudation rates (e.g., Bierman and Steig, 1996). In situ cosmogenic radionucleide concentrations, notably Beryllium-10 (^{10}Be), are now commonly measured to estimate the outcrop and basin-averaged denudation rates over geomorphi-

cally significant timescales (i.e., 10^3 to 10^6 years). Denudation rates measure the combined effect of physical (= erosion rate) and chemical (= weathering rate) processes (e.g., Von Blanckenburg, 2005).

Many basinwide ^{10}Be-derived denudation rate studies published in recent years strived to disentangle the complex interactions and feedbacks between climate, tectonic forcing, erosional and hydrological processes, lithology, and other environmental parameters (e.g., Norton et al., 2008; Meyer et al., 2010; Cyr et al., 2014; Scherler et al., 2014). Investigating the effect of climate on river incision is not trivial, as many nonclimatic factors such as lithology, vegetation, or tectonic processes can conceal potential climatic trends. Moreover, complex feedbacks may occur between climatic and nonclimatic phenomena governing long-term river incision (as an example, precipitation and vegetation cover are correlated to elevation, but elevation is also correlated to tectonic activity). Additional complications may include large-scale, long-term phenomena related to erosion (such as isostasy: (Bishop, 2007)), or geochemical factors including silicate weathering and the CO_2 cycle (Berner et al., 1983).

Most of these recent studies operate at the local scale and focus on site specificities. For instance, Ferrier et al. (2013) found a positive correlation between precipitation and river incision rates on a Hawaiian island. This study was made possible by the steep mean annual rainfall gradient observed on the island, combined with a limited lithologic variability. On the other hand, Riebe et al. (2001a) found that average denudation rates in the Sierra Nevada (California) did not correlate with climate despite the range of mean annual precipitation (20-180 cm/y) and temperature (4-15°C) dis-

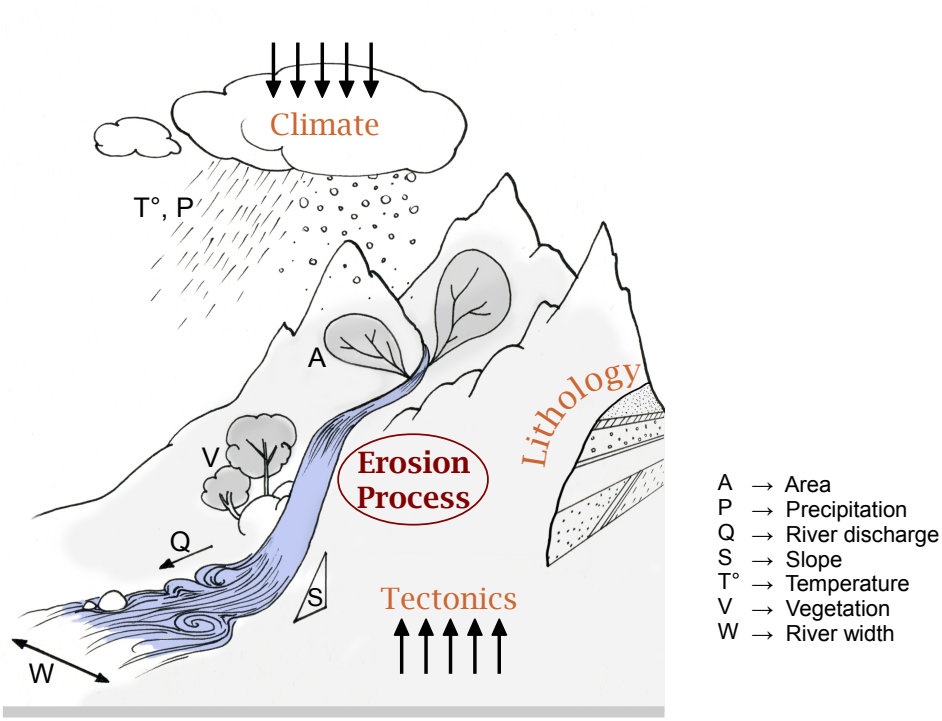

Fig. 1: Conceptual representation of the external and internal factors that modify bedrock rivers and their characteristics. Complex feedbacks operate between all the factors pictured. The balancing effect of climate, tectonics, and lithology on the erosion processes (affecting the river network as well as hillslopes) is central to our study.

played at the study site. D'Arcy and Whittaker (2014) pushed the analysis further by comparing six study areas spanning different climate zones. They deconvolved the tectonic and climatic variables first, removing the uplift signal included in orographic precipitation rates, and demonstrated a relationship between precipitation and channel steepness (often considered to be a proxy for erosion rate). A relationship between denudation rates and channel steepness is almost systematically observed (e.g., Kirby and Whipple, 2012), although here again covarying factors substantially complicate the interpre-

tation of data sets. For instance, Cyr et al. (2014) explained how changes in lithology affect the relationship between erosion and local steepness index. They argued that a negative correlation between denudation rates and channel steepness may be observed in areas of nonuniform lithology, whereas the opposite relationship may be true when lithology is uniform but rock uplift varies spatially.

Many of these studies contribute to the greater debate on the feedbacks between erosion and changing climate. Recent works (using thermochronometry) suggest that colder climatic conditions lead to increased mountain erosion (Herman et al., 2013; Thiede and Ehlers, 2013). This trend is partly explained by the high erosive efficiency of glacial and periglacial processes (Hales and Roering, 2007; Tucker et al., 2011; Andersen et al., 2015).

The stream power law, providing an expression for the erosion of fluvial systems, is extensively used to analyze and interpret the data sets. In its simplest form, it is formulated as (Howard and Kerby, 1983; Whipple and Tucker, 1999)

$$E = KA^m S^n \tag{1}$$

where E is the erosion rate ($[\mathrm{LT}^{-1}]$); K is an erodibility coefficient ($[\mathrm{T}^{-1}\mathrm{L}^{1-2m}]$) that encompasses the influence of climate, lithology, and sediment transport processes; A is the upstream drainage area ($[\mathrm{L}^2]$); and $S = -\partial z/\partial x$ is the local channel slope ([L/L]) with z the elevation. The drainage area is considered as a proxy for discharge (Wobus et al., 2006), therefore an averaged precipitation rate is included into the stream power law through the K term. The benefits, limitations, and alternatives of the stream power approach are

reviewed by Lague (2014). Although modifications to the stream power law have been proposed by many, including the role of varying channel width (e.g., Finnegan et al., 2005; Whittaker et al., 2007; Attal et al., 2008), sediment supply (e.g., Sklar and Dietrich, 2001a; Turowski et al., 2007; Hobley et al., 2011; Beer and Turowski, 2015; Aubert et al., 2016), or erosion thresholds (e.g., Lague et al., 2005; DiBiase and Whipple, 2011), Gasparini and Brandon (2011) found that many of these modifications could be collapsed into an equation of the form of Eq. (1).

The slope and drainage area exponents, respectively n and m, are empirical constants. Both of these values, as well as K, are major unknowns — although theoretical values of n ranging between 2/3 and 7/3 have been proposed by Whipple et al. (2000) based on the mechanics of river incision into bedrock. Recent studies have suggested that n values can exceed 2 when an erosion threshold (i.e., a critical shear stress must be exceeded for erosion to occur) is combined with specific distributions of large floods (Lague et al., 2005; DiBiase and Whipple, 2011). Whipple and Tucker (1999) showed that when erosion is proportional to specific stream power, $m = 0.5$ and $n = 1$. Many authors make this assumption and fix n to unity, while K remains unconstrained. This approach is partly because of the lack of data and partly because of the lack of a robust methodology to determine these two parameters. The variable n, being directly related to the degree of nonlinearity between the stream incision rate and specific stream power, carries information about the physics of the dominant erosion process. Whether its value is greater or less than one has a strong impact on the evolution of river profiles

(Whipple and Tucker, 1999; Tucker and Whipple, 2002), especially in transient landscapes where n controls the propagation of knickpoints along the river network.

Equation (1) can be rewritten as

$$S = \left(\frac{E}{K}\right)^{1/n} A^{-m/n} \tag{2}$$

which may be identified with Hack's observation that most river profiles at equilibrium are correctly described by a power-law relationship between S and A such as :

$$\begin{aligned} S &= k_s A^{-\theta} \\ k_s &= \left(\frac{E}{K}\right)^{1/n} \\ \theta &= m/n \end{aligned} \tag{3}$$

where θ is referred to as the concavity index and k_s as the channel steepness index (Hack, 1957; Flint, 1974). This relationship is only valid above a critical threshold drainage area, typically ranging between 0.1 and 5 km^2 (Wobus et al., 2006), below which debris flows dominate over fluvial processes (Stock and Dietrich, 2003). This transition separates uphill zones where slopes are largely invariant with increasing drainage area from downhill zones where slopes decrease systematically downstream (Wobus et al., 2006). In theory, Eq. (3) holds only for river profiles developed in areas of uniform climate, lithology, and rock uplift. Field and map data (e.g., Howard and Kerby, 1983; Slingerland et al., 1998) as well as theoretical developments based on the stream power incision model (Whipple and Tucker, 1999), predict that θ falls within a relatively narrow range ($0.4 < m/n < 0.6$). The

concavity index should be independent of the erosion process and thresholds. In uniform uplift and lithology settings, θ should only depend on the relationships between discharge and drainage area and between channel width with discharge (Whipple and Tucker, 1999).

The steepness index k_s is a measure of channel slope normalized for the upstream drainage area (Wobus et al., 2006). Its value and that of θ can be determined with a linear regression of channel slope against drainage area on a log-log plot (Eq.3). However, k_s and θ being strongly correlated (Wobus et al., 2006), the steepness index needs to be normalized ($k_{s,ref}$) with a reference concavity (θ_{ref}) for comparison purposes (Whipple, 2004). This procedure relies on the observation that, contrarily to the concavity index, k_s may vary with rock uplift rate, climate, and lithology (Kirby and Whipple, 2001; Wobus et al., 2006). The units of the steepness index depend on θ (k_s $[L]$ for $\theta_{ref} = 0.5$).

Equation (2) is the foundation of the slope-area analysis, a method frequently used to infer erosion patterns in bedrock river profiles. Rock uplift can then be estimated by assuming that the topography is at steady-state ($\partial z/\partial t = 0$) with uniform K, identifying $E = U$ (Stock and Montgomery, 1999; Kirby and Whipple, 2001; Wobus et al., 2006; DiBiase et al., 2010; Kirby and Whipple, 2012). If a given river profile does not follow such a power law, it may be experiencing spatial or temporal changes in uplift rates, variations in bedrock lithology, or transitions in erosion or transport mechanisms.

The only global scale ^{10}Be compilations available make no mention of the

stream power law or its parameters, focusing on the denudation rate and its dependence on climate, lithology, or tectonics (Von Blanckenburg, 2005; Portenga and Bierman, 2011; Willenbring et al., 2013a). Handpicked data sets from a variety of localities have been compared, mostly to comment on the reproducibility of the positive relationship between basin-averaged denudation rates and the normalized steepness index (e.g., Kirby and Whipple, 2012). Here, we present the first global scale compilation of the stream power law's parameters that allows for multiple-site analysis. Our extensive data set is the result of the systematic analysis of previously published basinwide denudation rates in bedrock rivers. We collated 1457 samples from 77 publications, standardized the denudation rates, and augmented the data set with basin-averaged environmental parameter information such as mean annual temperature and precipitation, basin area, or the percentage of vegetation cover.

We aim to use this data set to explore how lithology, climate, and tectonics influence stream power law parameters (m/n, n, and K) at the global scale. In the first section, the data normalization and methods are described. We explain how the variables n, m/n, K and the steepness index are calculated using the integral method of channel profile analysis developed by Perron and Royden (2013). Secondly, we analyze the results, focusing successively on the influence of climate, lithology, and tectonics on the stream power law parameters. Bivariate plots, boxplots, and a multiple regression are used to study the data set and the relationships between variables. In a third section we discuss the limits of the data set and how data repartition, scale, and other issues may affect the results. Our analysis demonstrates that in most

cases, the channel slope of a river does not reflect a simple specific stream power model for fluvial erosion and that erosional thresholds are required to explain the observations. We also demonstrate that river channel gradients do not correlate with precipitation. These results fundamentally question the application of the stream power model, as it has become common practice to systematically employ a simplified, linear version of the model with $n = 1$ and $m/n = 0.5$.

2. Data and methods

2.1. Data selection and standardization

We compile previously published ^{10}Be basinwide denudation rates (Figure 2 + supplemental material). A total of 1457 samples were collected from the literature and similar compilations (Portenga and Bierman, 2011; Willenbring et al., 2013a). These data points are gathered into 59 study areas (which we henceforth call *zones*) that may combine more than one source of data. Overall, we have striven to define study zones that displayed the maximum number of samples combined within a geographically restricted area so that the environmental characteristics of each zone may be as uniform as possible.

Comparison of denudation rates from ^{10}Be across multiple studies is a challenge because a wide range of methods are used to calculate these rates. For example, five different cosmogenic production schemes are commonly used in the literature (e.g., Lal, 1991; Dunai, 2000; Stone, 2000; Desilets and Zreda, 2003; Lifton et al., 2005). Some authors do not consider topographic shielding, whereas others use a variety of reported shielding schemes (e.g.,

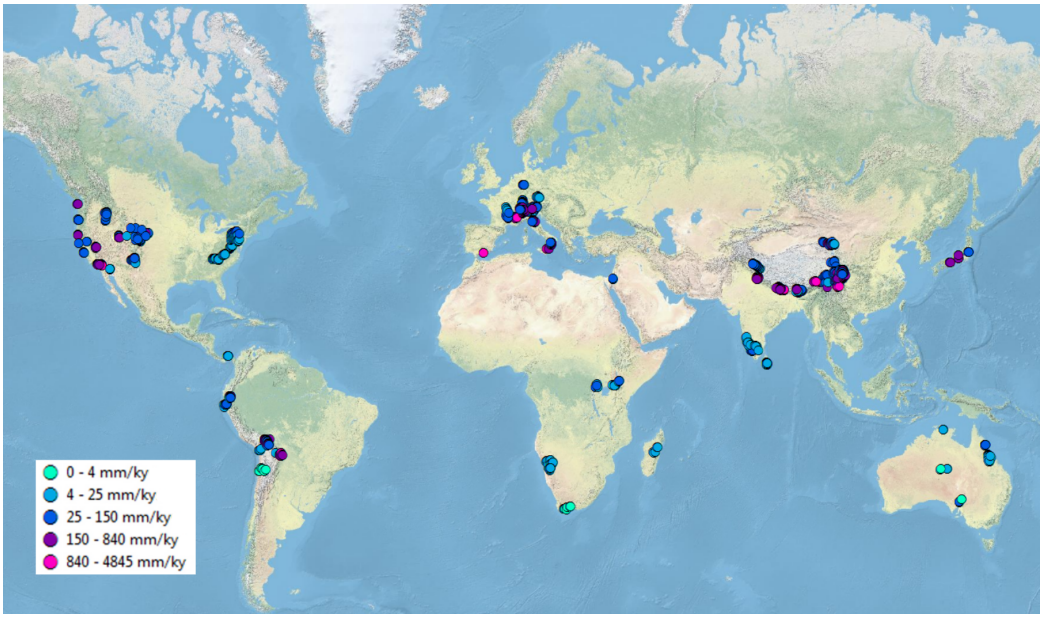

Fig. 2: Geographical distribution of basinwide denudation rate samples (see Supplementary material for data table and the list of source publications). Symbols show the denudation rates, recalculated for standardization.

Dunne et al., 1999; Codilean, 2006; Norton and Vanacker, 2009). Estimated production rates of ^{10}Be at sea level and high latitude, which are used to scale production at other locations, have changed significantly over the last 15 years as more calibration sites are reported. For example, Stone (2000) reported that a value of 5.1 atoms.g^{-1}.y^{-1} has been used, whereas the current estimate is closer to 4.3 atoms.g^{-1}.y^{-1} (from COSMOCALC, Vermeesch (2007), ver. 2.0). Finally, production of ^{10}Be by muons is highly uncertain, with a variety of schemes used in the literature (e.g., Granger and Smith, 2000; Heisinger et al., 2002a,b; Braucher et al., 2011).

To allow comparison between studies, we have recalculated all 1457 samples using a common method. We have extracted sampled basins from

the 2000 Shuttle Radar Topography Mission data (SRTM), which can be downloaded from http://earthexplorer.usgs.gov/. All ^{10}Be concentrations have been normalized to the Nishiizumi et al. (2007) standardization using the ratios reported by Balco et al. (2008). We use the Lal/Stone scaling method (Lal, 1991; Stone, 2000), with production rates of ^{10}Be set to 4.3 atoms.g^{-1}.y^{-1} (from COSMOCALC, Vermeesch (2007), ver. 2.0). Production rates are calculated on a pixel-by-pixel basis, with atmospheric pressure at each pixel calculated using interpolation of the climate reanalysis of Compo et al. (2011), following the approach of Balco et al. (2008). Production of muons is based on the scheme of Braucher et al. (2011), as implemented in COSMOCALC version 2 using four exponential functions. The half life of ^{10}Be is set to 1.387 My based on Chmeleff et al. (2010) and Korschinek et al. (2010). Topographic shielding is calculated based on Codilean (2006), using a zenith spacing of 5° and an azimuth spacing of 8°. Snow shielding values are taken from values reported in the original studies.

For each sample in the table, basin-averaged parameters are calculated based on published global maps. Basin area and elevation are derived from the DEM, and mean annual precipitation (MAP) and temperature (MAT) come from a continuous, spatially interpolated data set at a 1-km resolution (Hijmans et al., 2005). Following the approach of Portenga and Bierman (2011), we use the Global Seismic Hazard Assessment Program (GSHAP) map of peak ground acceleration developed by Giardini et al. (1999) as a proxy for seismicity. Seismicity is defined as a magnitude of ground motion with a 10% chance of being exceeded within 50 years. The 59 zones are divided into five climate categories (tropical, arid, temperate, cold, and po-

lar) based on the Koppen-Geiger climate classification system (Peel et al., 2007). When a zone covers more than one type of climate, the dominant climate group is chosen. Similarly, four lithology categories (igneous, metamorphic, sedimentary, and mixed) are assigned to a given zone based on the information provided in each publication.

We also record the mean percentage of vegetation (tree cover) within a basin from a 1-km resolution data set by DeFries et al. (2000). The values in the data set range from 10 to 80%. Specific values indicating a 0-10% tree coverage and nonvegetated areas are replaced by cell values of 5% and 0%, respectively.

The complete data set can be found in the supplemental materials. The data table also mentions whether basins are or probably were previously glaciated (from the original publications). Data preparation and post-treatment scripts may be downloaded at https://github.com/LSDtopotools/.

2.2. Integral method of channel profile analysis

The integral method is an alternative approach to slope-area analysis that was introduced by Royden et al. (2000) and further developed by Perron and Royden (2013). By integrating the stream power equation (Eq.1), the river profile's horizontal coordinate is transformed into a variable $\chi[L]$, which is simply the upstream distance normalized for drainage area. The main advantage of this method is the reduction of the influence of the noise associated with topographic data (see Perron and Royden (2013) for a detailed discussion of the advantages and potential drawbacks).

If we consider a simplified setting where E and K are constants in space and time, we can rewrite Eq. (2) and integrate it upstream from a base level

x_b as follows:

$$S = -\frac{dz}{dx} = \left(\frac{E}{KA^m}\right)^{1/n} \tag{4}$$

$$\int dz = \int \left(\frac{E}{KA^m}\right)^{1/n} dx \tag{5}$$

$$z(x) = z(x_b) + \left(\frac{E}{K{A_0}^m}\right)^{1/n} \chi \tag{6}$$

$$\text{with} \qquad \chi = \int_{x_b}^{x} \left(\frac{A_0}{A(x)}\right)^{m/n} dx \tag{7}$$

and A_0 is a reference drainage area. In a transformed profile called χ-plot (Fig. 3), a channel or a series of channel segments that obey Eq. (4) plot as a straight line whose slope is a function of the ratio E/K raised to the power $1/n$. The χ value depends on the unknown concavity index (m/n). The integral method provides two independent tests to estimate the best m/n ratio. If a river profile (made of one or more channel segments) obeys Eq. (4) and features uniform K and E, then (i) individual channels should be linear in χ-elevation space and (ii) all channels in the network should be collinear. In other words, the correct m/n value should collapse the mainstream and its tributaries into a single line (Perron and Royden, 2013). The collinearity of the tributaries is a consequence of the coordinate transformation, as points with similar elevations should have similar values of χ (providing that K and E are uniform), regardless of their drainage area.

2.3. Estimation of m/n, n, and K

In the following, a data point corresponds to a value of ^{10}Be denudation rate, which is also related to a geographical position in the basin (latitude, longitude). We call junctions the points of the channel network where mainstem and tributaries connect. For the analysis, data points are assimilated

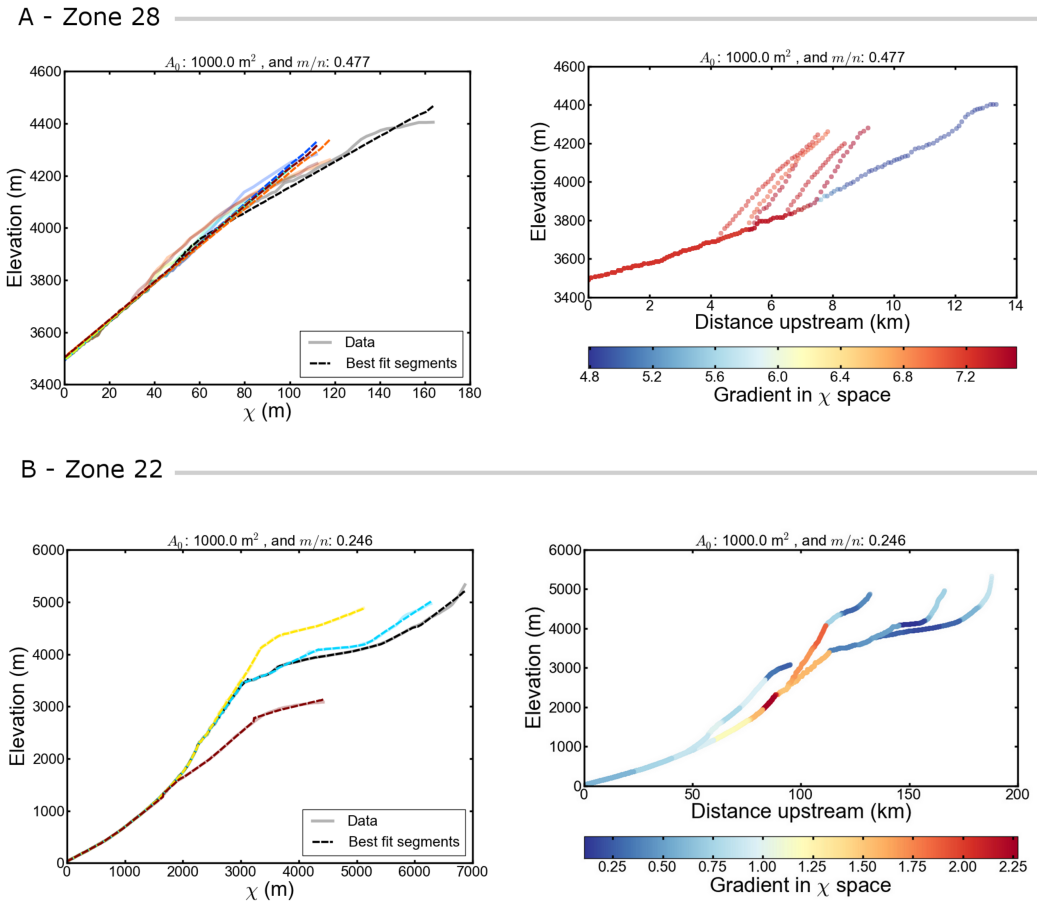

Fig. 3: Example profiles of a mainstem channel and tributaries associated to two denudation rate samples. (A) An ideal χ-plot (left) and the elevation against upstream distance for a sample from zone 28 (Himalaya). (B) The χ-plot (left) and the associated profile (right) for a sample in zone 22 (Andes) that requires more analysis.

to their nearest junction and are associated to the corresponding drainage basin (the portion of the upslope basin draining into this point). The best m/n value is estimated for a given zone by carrying a sensitivity analysis on three representative data points (and their associated basins) in the zone. Once the best fit m/n value is selected, all samples in the zone are used to

derive the steepness index, slope exponent, and erodibility. The details of the method are given below.

Mudd et al. (2014) proposed a statistical approach to determine the most likely piecewise linear fit to a channel profile in χ-elevation space. The associated code provides a reproducible method to estimate the best concavity index based on the digital elevation model of an area. The full approach is described in detail in Mudd et al. (2014) and the code available online at $https://github.com/LSDtopotools/LSDTopoTools\_ChiMudd2014$. To analyze our data set, for each of the 59 zones we use this code to extract the drainage network from the DEMs. The drainage network extraction is based on an area threshold value (equal to $A_0 = 1000\ m^2$), that is we assume that the channel head starts at this given drainage area threshold. The junctions nearest to each cosmogenic nuclide data point are selected manually to ensure that the sample point is placed upon the sampled channel as represented in the DEM. A sensitivity analysis is then performed on three representative junctions for each zone, in order to test the effect of changing the model parameters following Mudd et al. (2014). The three junctions are handpicked to make sure that the sensitivity analysis is performed in the best conditions (large basin area, located within clusters of samples). We obtained 81 m/n values (27 values for each junction) for both the fit of mainstem and the collinearity of tributaries tests (Fig. 4A) within each zone. We chose to select the mean concavity index based on the collinearity test as best estimator for a given zone based on our extensive testing of the Mudd et al. (2014) method and on the recommendations of Perron and Royden (2013). The error on m/n is the standard deviation associated with this sensitivity

analysis.

Notably, the steady-state hypothesis frequently adopted in this framework in order to infer rock uplift patterns (by replacing E by U: Kirby and Whipple (e.g., 2012)) is not necessary and has not been used in the present work. Royden and Perron (2013) demonstrated that even in cases of transient channel incision, the slope in χ-space will reflect local erosion rates. Although Hack's law is based on the hypothesis that the river profile is at equilibrium, this relationship is only applied to sections of the profile. Our segment-fitting method (Mudd et al., 2014) uses piecewise fits of channel segments so extracting the m/n value is possible whether or not the entire river profile is at equilibrium.

Knowing the m/n ratio, the slope of the profile in χ-space, called M_χ, can be extracted from the code for each data point. When the χ-profile is made of more than one tributary, the M_χ value is estimated as the average of the mainstem and tributary slopes. This slope is the equivalent of the steepness index in the integral method framework and expressed as

$$M_\chi = \left(\frac{E}{K A_0^m} \right)^{1/n} \tag{8}$$

The steepness index, k_s, and M_χ are closely related, as M_χ is simply k_s multiplied by the constant $A_0^{-m/n}$. The identity $k_s = M_\chi$ is true if $A_0 = 1$ m^2. According to Eq. (8), plotting M_χ against the denudation rate E in log-log space should result in a line whose slope and intercept are related to n and K, respectively, such as

$$log_{10}(M_\chi) = \frac{1}{n} log_{10}(E) - \frac{1}{n} log_{10}(K A_0^m) \tag{9}$$

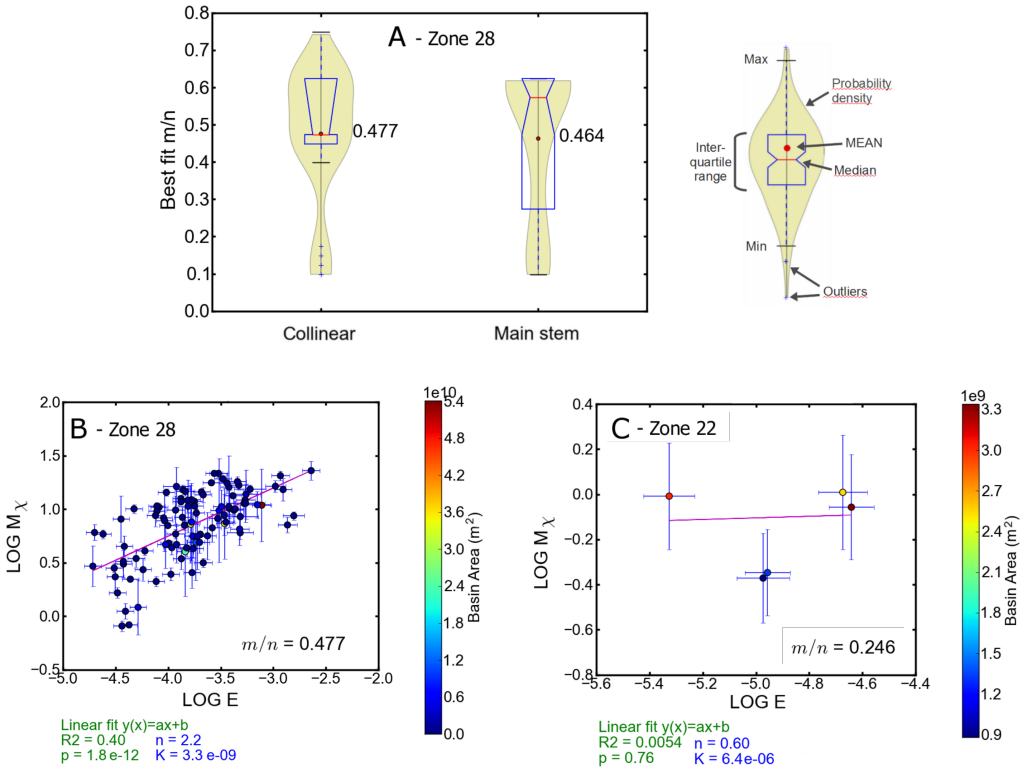

Fig. 4: Examples of plots generated for the estimation of the stream power law parameters. (A) and (B) are the results obtained for zone 28, an ideal case; while (C) illustrates a poor fit (zone 22). (A) Collinear and mainstem-based estimations of m/n generated by the sensitivity analysis (81 values in total, three for each junction in the given zone). (B) and (C) Denudation rate against mean steepness index in log-log scale, with linear regression, for the estimated m/n value.

Using a simple linear regression tool in Python, we derive n and K from the M_χ against E plots for each zone. Because this linear regression is very sensitive to outliers, we obtain a more robust estimation of n and K by bootstrapping the data set. For a given zone, the method described above is repeated j times for a data set of size j, where each data point is excluded

once. Therefore, we obtain $j+1$ values of n (j values for partial data sets and one value for the entire data set). We chose not to exclude more than one point at a time because many data sets are critically small (47.5% of the zones have < 15 points). The best estimator for the slope exponent, $\bar{n}$, is the mean of the $j+1$ values of n obtained by bootstrapping. Its error is quantified by the standard deviation.

The best K estimator is then calculated by inverting Eq. (8) with the $\bar{n}$ value such as

$$\bar{K} = \frac{1}{j} \sum_{j} \frac{E_k}{A_0^{m/n} {M_{\chi,j}}^{\bar{n}}} \tag{10}$$

The quality of these estimations is quantified by the p value. This parameter measures the probability that the observed effect occurred by chance alone. A result is considered statistically significant when p is less than a given threshold. We decided to subset the data based on criteria of $p \leq 0.16$ using the average p value ($\bar{p}$) from the bootstrapping, thus rejecting 26 zones out of 59. To simplify the notations, $\bar{n}$ and $\bar{K}$ are still denoted n and K in the following.

2.4. Constrained subset and normalized K

The slope exponent n, erodibility K, and steepness index M_χ each depend on the concavity index. As all zones have different m/n values, comparing n and K between zones can be challenging. The usual solution to this problem is to normalize M_χ and K by arbitrarily fixing the concavity index. We chose the reference value $m/n_{ref} = 0.5$ based on the literature (Kirby and Whipple, 2012; D'Arcy and Whittaker, 2014) and our own results. The bootstrapping technique described above has been reproduced with the m/n_{ref} value for

the constrained subset exclusively ($\bar{p} \leq 0.16$). Therefore, in the following, m/n and n values are calculated for the constrained subset (varying m/n), whereas K and M_χ are derived from the constrained subset with a fixed m/n_{ref} (denoted K_{ref} and $M_{\chi,ref}$).

2.5. Statistical methods

The denudation rate, steepness index, area, and the erodibility coefficient vary over several orders of magnitude, so a base 10 log-transformation was applied to these variables. Bivariate analysis is used to observe the influence of environmental parameters (MAP, MAT, basin area, elevation, seismicity-PGA, percentage of vegetation, latitude), $M_{\chi,ref}$, and E on the stream power law parameters (m/n, n, and K_{ref}). Violin plots (boxplots showing the normalized probability density function of the sample) that display the mean and the median (robust measure of the cenral tendency) give an overview of the parameters and their variations between categorical variables (Fig. 6 and Fig. 4A for a description of violin plots). The data set is categorized into climate zones (arid, tropical, temperate, cold and polar, based on the Koppen-Geiger climate classification (Peel et al., 2007)), general lithology (igneous, metamorphic, sedimentary and mixed) and tectonic activity (active or inactive). The seismically active areas have an average Peak Ground Acceleration (PGA) above 2, meaning that a magnitude 2 earthquake can be expected within 50 years (Portenga and Bierman, 2011).

A multiple regression (linear, backward stepwise, see Table 1) is performed using the R statistical software (*lm* and *stepAIC* functions). The concavity index, n, and K_{ref} are successively chosen as predicted variables. We applied weights equal to the inverse of the number of samples in each

zone. That way we give less weight to large zones (many samples) and more weight to basins belonging to small zones, as a means to reduce serial correlation. We carefully selected the variables included in the analysis in order to reduce collinearity. Indeed, a multiple regression becomes meaningless when two or more predictors show a high degree of correlation. For this reason, we only considered the mean annual temperature and precipitation, area, vegetation, latitude, and seismicity and ignored elevation, steepness index, and other interfering variables. If $M_{\chi,ref}$ is included in the predictors, similar coefficients are obtained for the remaining variables and all predicted variables show a high correlation with $M_{\chi,ref}$ (as is expected given Eq. 8). This restricted list of predictors explain the low adjusted R^2 values. Another issue is the dependence of the coefficients on the sample size. Subgroups or categories with many samples are more likely to feature high coefficients, thus creating a bias when comparing different subsets. There is no easy remedy to this problem, and its consequences are discussed in section 4.

3. Results and discussion

3.1. Global analysis

Figure 5 (D, E, F) shows a clear positive correlation between normalized steepness index ($M_{\chi,ref}$) and denudation rate. This relationship was observed at the global scale by Kirby and Whipple (2012), who compared several data sets from across the world. Here we confirm this trend for a wider range of landscapes. Even when considering the full (Fig. 5A) or $\bar{p} \leq 0.16$ subset (Fig. 5B) non-normalized data, the correlation between M_χ and E is still obvious. The correlation becomes stronger for $M_{\chi,ref}$, as is expected as these

zones are selected based on the goodness of fit for a linear regression between $log_{10}(M_{\chi,ref})$ and $log_{10}(E)$ (see section 2.3). However, we feel confident that this data subset remains a good representation of the field studies as a whole, as most of the rejected zones were rejected due to lack of data (Fig. 4). Indeed, more than 47% of the zones have < 15 samples in the global data set, of which only six zones (about 18%) appear in the $\bar{p} \leq 0.16$ subset.

Figure 6 displays a very skewed denudation rate distribution, reflecting the wide range of environments and processes gathered in the data set. The highest denudation rate, $max(E) = 5655$ mm/ky, is observed in Nepal (zone 56, partially glaciated; Godard et al. (2012)). For the subset data, we find $< E >= 242 \pm 59$ mm/ky.

In contrast, the concavity index is relatively well constrained, with mean and median values falling between 0.5 and 0.52 ($< m/n >= 0.51 \pm 0.12$). This observation corroborates the previous predictions of Whipple and Tucker (1999). As can be seen in Fig. 6, we did not test values of m/n above 0.65; therefore a wider range of θ may have been observed, although the mean and median probably would not be significantly affected given the distribution of the data, as shown by the probability density function. Table 1 shows that, at the global scale, the concavity index is relatively insensitive to all environmental parameters tested (MAT, MAP, basin area, vegetation, latitude, and seismicity). This is in agreement with the findings of Hack (1957) and Whipple and Tucker (1999), which suggest that m/n only depends on the relationships between drainage area, discharge, and channel width. According to our multiple regression analysis, basin area and precipitation (proxy for discharge) do not influence m/n significantly when considered independently.

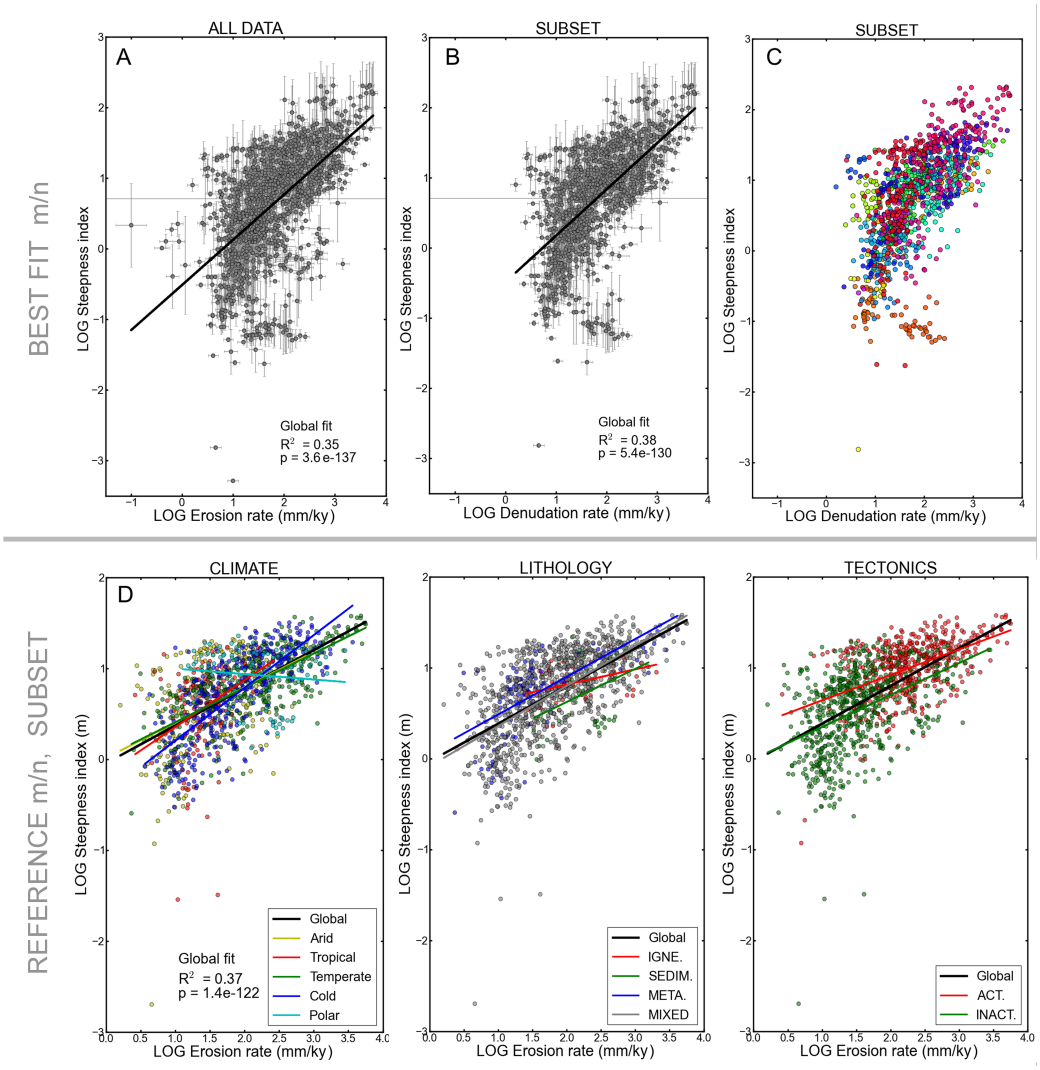

Fig. 5: Channel steepness, M_χ, against denudation rates E in log-log scale. (A) and (B) The nonnormalized full and $\bar{p} \leq 0.16$ subset data, respectively, with error bars. (C) The same subset with symbol colors identifying the different zones. On the second row, (D), (E), and (F) the $\bar{p} \leq 0.16$ subset data with fixed $m/n_{ref} = 0.5$, showing specific colors and linear regressions for each category under the climate, lithology, and tectonics subgroups, respectively.

Figure 6 shows an important result: the mean slope exponent observed at global scale is well above one, with $< n >= 2.6 \pm 0.4$. Despite the relatively wide range of n values displayed, the consistency between the mean and the median suggest that n is, on average, greater than unity.

The multiple regression analysis (Table 1) shows that the seismicity-PGA and the MAT are powerful regressors on n. The respective positive (seismicity) and negative (MAT) correlations with n have been previously predicted based on theoretical considerations, but this hypothesis has never been tested. Molnar et al. (2007) suggested that the slope exponent, being a measure of the non-linearity of the incision processes, will be high in tectonically active settings where slope changes and rock fracturing due to stress are expected. On the other hand, frost cracking and spallation in areas featuring low temperatures are responsible for rock weathering (Delunel et al., 2010). These processes are triggered at specific temperature thresholds and potentially contribute to a higher slope exponent n.

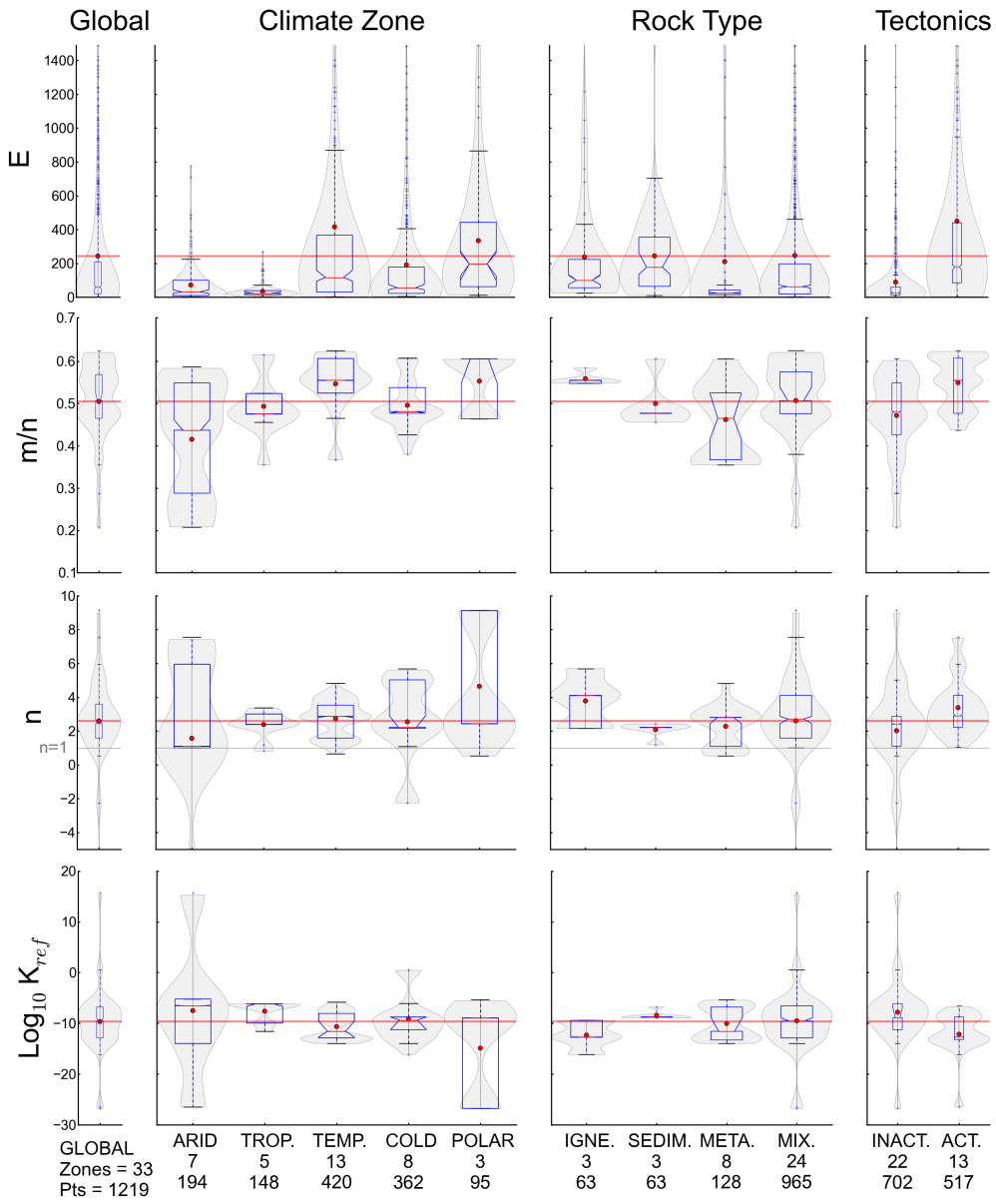

Fig. 6: Violin plots for the denudation rate E (in mm/ky), m/n, n and K_{ref} (rows), given for the entire $\bar{p} \leq 0.16$ subset data (first column), and in the subsequent columns climate, lithology and tectonic sub-categories. Violin plots are boxplots superposed on the probability density function of the sample (in grey). Mean values are marked by round red symbols, medians are red segments (part of the boxplot). See Fig. 4 for a graphic description of a violin plot. Mean values of the four parameters appear as a red line spanning all the columns. The critical value $n = 1$ is highlighted in grey (line). The number of zones and number of samples in each sub-category is indicated at the bottom.

The erodibility coefficient is, however, far less constrained at the global scale (Fig. 6). This variability is anticipated, and to the authors' knowledge this is the first tentative quantification of K for such an extensive data set. We obtain an average value of $< K_{ref} >= 1.2*10^{14} \pm 3.9*10^{14}$ ($[T^{-1}L^{1-2m}]$), but in that case a more robust measure is given by the median with $2.9*10^{-10} \pm 1.0 * 10^{-9}$. Let us remark that although the mean and median are very close in Fig. 6, they relate to $log_{10}(K_{ref})$ and not K_{ref}. Unlike the mean, the median is not affected by the log_{10} transformation (the log_{10} transformation of the mean is different from the mean of the log_{10} transform). This explains why the mean and median for K_{ref} are so dissimilar. This discrepancy between mean and median is mostly a consequence of zone number 4, which features a suspect value of K above $4 * 10^{15}$ ($[T^{-1}L^{1-2m}]$). The median value of normalized erodibility is lower than the $10^{-2} - 10^{-7}$ $m^{0.2}/y$ range reported by Stock and Montgomery (1999); but given the high variability of K in our data, the result seems to be consistent with the previously published values. We must point out that K is the most difficult stream power law parameter to estimate, as is reflected by the large errors associated with its measure.

3.2. Influence of climate

It is difficult to isolate clear climatic trends when looking at Fig. 6, as most boxplots overlap. This lack of climate response is also reflected in Fig. 5, where linear regressions between $M_{\chi,ref}$ and E for the five climate categories (except polar areas) have similar slopes and intercepts (which are directly related to n and K, respectively). We may safely suggest, however, that arid climates lead to higher erodibility and lower slope exponent. Arid regions indeed feature lower n and higher K medians (Fig. 6) compared to

other climates. Arid zones are scarcely vegetated, as shown in the supplementary material, and thus more vulnerable to extreme events (Coppus and Imeson, 2002). It has been suggested that the landscape alteration in arid zones is more controlled by the absence of landscape recovery than by the absolute magnitude of the events. Indeed, tropical zones are characterized by intense and frequent storms, but those are combined with very fast recovery rates thanks to vegetation repopulation (Wolman and Gerson, 1978). On the the other hand, the high magnitude events taking place in arid zones are rare and clearly diverge from the average meteorological conditions usually encountered in these areas (Slater and Singer, 2013). These factors would explain a high erodibility of soils and bedrock combined with the absence of threshold-controlled incision processes in arid environments (see below).

We also observe a high denudation rate signal (median) for polar zones compared to other climate regions (Fig. 6), but it is not associated with extreme values of n and K as we may have expected. Unlike arid climates, polar zones are mostly characterized by high denudation rates and low temperatures (where arid zones mainly feature low MAP and scarce vegetation). Frost cracking (rock breakdown caused by expanded freezing water in rock porosity) is probably the most important weathering process in polar zones. It operates most effectively at temperatures around -3°C to -10°C (Walder and Hallet, 1985; Anderson, 1998; Hales and Roering, 2007), which falls clearly into the polar MAT range displayed in the supplemental material. These threshold (temperature) processes could explain the slightly skewed distributions of K_{ref} (below average) and n (above average) observed in polar zones (Fig. 6).

Table 1: Results of the multiple (backward stepwise) regression performed for m/n, n and K_{ref} (rows, $[T^{-1}L^{1-2m}]$) for the global data subset (first column), climate, lithology and tectonic sub-categories (following columns).

		GLOBAL	CLIMATE					LITHOLOGY				TECTONICS	
Predicted	Predictors		ARID	TROP.	TEMP.	COLD	POLAR	IGNE.	SEDIM.	META.	MIX.	INACT.	ACT.
m/n	MAT	-6.4E-03	-1.2E-02	-1.5E-02	3.4E-03	-2.7E-03	1.2E-02	3.6E-03	-	-	-6.5E-03	-8.3E-03	7.9E-04
	MAP	4.6E-05	7.5E-05	1.8E-05	-1.5E-05	-	2.0E-04	1.3E-04	1.0E-04	2.9E-05	5.1E-05	4.3E-05	5.5E-05
	Log10 Area	-1.5E-02	-	-1.5E-02	7.8E-03	-1.1E-02	-7.5E-03	-	-	-1.4E-02	-1.5E-02	-1.5E-02	-
	% Vegetation	5.9E-04	2.4E-03	-2.9E-03	-1.3E-03	3.9E-04	3.3E-04	-5.8E-04	2.1E-04	-2.5E-03	1.5E-03	1.1E-03	-2.9E-04
	Latitude	-1.2E-03	-4.6E-03	-2.8E-03	1.4E-03	-3.1E-03	-2.1E-02	-	3.6E-03	2.3E-03	-1.9E-03	-1.6E-03	2.6E-04
	Seismicity PGA	3.0E-02	8.3E-02	-6.6E-02	4.8E-03	2.1E-02	-	-5.8E-03	-1.2E-02	-3.3E-02	3.6E-02	1.9E-02	-
	Adj R^2	0.3066	0.7589	0.6495	0.3026	0.286	0.7784	0.6471	0.9541	0.5715	0.4684	0.2738	0.2567
n	MAT	-1.8E-01	-5.5E-01	-1.9E-01	2.1E-02	1.3E-01	-5.1E-01	2.8E-01	-	-	-2.5E-01	-1.5E-01	-7.2E-02
	MAP	1.0E-03	-2.7E-03	-	-7.1E-04	1.0E-03	-9.4E-03	9.4E-03	-6.1E-05	2.4E-03	1.2E-03	1.4E-03	-1.1E-03
	Log10 Area	-2.1E-01	-4.0E-01	-1.7E-01	1.7E-01	-	4.0E-01	-	-	1.3E-01	-2.4E-01	-	-3.8E-01
	% Vegetation	7.5E-03	-9.0E-02	-2.8E-02	1.1E-02	-	-2.2E-02	-4.0E-02	-4.0E-04	-7.7E-03	1.8E-02	2.6E-02	-
	Latitude	-2.4E-02	-2.0E-01	1.0E-02	-2.2E-02	-4.6E-02	1.4E+00	-2.9E-01	1.9E-02	2.8E-02	-4.0E-02	-3.1E-02	2.8E-02
	Seismicity PGA	5.3E-01	1.9E+00	-1.2E+00	3.2E-01	5.4E-01	8.4E-01	-7.3E-01	1.2E-02	1.1E+00	5.2E-01	6.8E-01	-2.3E-01
	Adj R^2	0.1575	0.6215	0.7166	0.4496	0.1538	0.8664	0.7365	0.9995	0.5805	0.2	0.1608	0.54
Log_{10} K_{ref}	MAT	5.4E-01	1.5E+00	5.6E-01	1.4E-01	-2.7E-01	1.5E+00	-5.5E-01	-	-	7.3E-01	4.7E-01	2.6E-01
	MAP	-2.5E-03	8.6E-03	3.5E-04	-4.9E-04	-	2.5E-02	-1.9E-02	3.2E-04	-5.9E-03	-2.8E-03	-3.3E-03	1.6E-03
	Log10 Area	3.7E-01	-	2.2E-01	-5.9E-01	-	-1.1E+00	-	-	-5.9E-01	4.5E-01	-	5.2E-01
	% Vegetation	-3.6E-02	2.2E-01	3.7E-02	-4.8E-02	-	4.2E-02	7.9E-02	1.2E-03	-	-5.3E-02	-8.1E-02	-
	Latitude	9.2E-02	5.6E-01	3.9E-02	8.3E-02	1.4E-01	-3.5E+00	5.3E-01	-3.0E-02	-8.0E-02	1.3E-01	1.1E-01	-4.7E-02
	Seismicity PGA	-1.4E+00	-5.0E+00	3.0E+00	-9.7E-01	-1.6E+00	-	1.4E+00	-4.7E-02	-2.8E+00	-1.5E+00	-2.2E+00	5.8E-01
	Adj R^2	0.1954	0.6648	0.5692	0.422	0.2266	0.8529	0.7197	0.9978	0.5573	0.2565	0.1989	0.4055
	Nb of points =	33	7	5	13	8	3	3	3	8	24	22	13
	Nb of zones =	1219	194	148	420	362	95	63	63	128	965	702	517

The table shows the regression coefficients associated with each predictor variable: mean annual temperature (MAT, Celsius), mean annual precipitation (MAP, mm), basin area (m^2, in log10), percentage of vegetation, latitude, and seismicity (Peak Ground Acceleration). Darker colors are associated with higher absolute coefficient values, highlighting strong correlations between predictor and predicted variables. Only coefficients in bold are statistically significant (i.e., their p-value is below 10^{-3}). Adjusted R^2 values indicate the goodness of fit, and the number of zones and samples for each subcategory are shown at the bottom of the figure.

The multiple regression analysis (Table 1) shows that K_{ref} is most sensitive to the mean annual temperature and the seismicity at the global scale. However, the signs of the coefficients are both unexpected, and it is unclear

when looking at the bivariate plots (supplemental material) whether or not these trends can be fully trusted. Table 1 shows that K_{ref} is expected to be positively correlated to MAT and anticorrelated to seismicity. The relation between MAT and K_{ref} may be explained by specific processes taking place in arid zones, such as rock failure or salt cracking (salt expands in rock fractures under temperature gradients, weakening the rock; Smith et al. (2005); Eppes et al. (2010)). The observation that K decreases with an increase in tectonic activity is surprising, but may be the result of interactions and feedbacks between parameters (see section 3.4). Given the high degree of uncertainty associated with the estimation of K and the multiple regression itself, we would rather not overinterpret the results.

Weaker K relationships with basin area, latitude, and the percentage of vegetation are also observed. The negative correlation between erodibility and vegetation is expected, as vegetation and root systems are known to stabilize the soil structure and shield it from splash processes, prevent bank failure, and overall reduce erosion and sediment transport (Collins et al., 2004). Given this result, we understand that the potential weathering effect of root systems on bedrock is counter-balanced by the overall shielding and stabilizing effects of vegetation. Vegetation is also an important factor in landscape recovery after extreme events, thus supporting the negative correlation with K (Wolman and Gerson, 1978).

The relationship between the erodibility coefficient and latitude (proxy for climate) suggests that K may show some sensitivity to climate. However, the main result here is the absence of correlation between the mean annual precipitation (MAP) and K, when theory predicts that K is a function of

discharge and, by extension, precipitation. Again, we should exercise caution given the nature of the data set. Such a relationship may exist but not appear in the analysis at this point because too many parameters vary simultaneously. Additionally, important elements may be missing from our approach. For instance, it would be interesting to include storminess or rainfall intensity; unfortunately these variables are extremely hard to reconstruct in the past (DiBiase and Whipple, 2011).

3.3. Influence of lithology

Figure 6 shows that igneous rocks are often associated with high slope exponents and low erodibility compared to other types of rocks. As shown by the relatively low denudation rate, granitic rocks stand apart as stronger formations that get predominantly eroded by means of frost cracking or rock fracturing in seismically active zones. Such processes may be less frequent but are more efficient compared to chemical, water, and wind erosion or other commonly observed weathering processes (Riebe et al., 2001b). Table 1 supports this idea, showing a distinct effect of temperature and seismicity on n and K for granitic rocks. The fact that latitude also appears as a strong regressor for n and K suggests that climate plays an important role on erosive processes in landscapes where igneous substrate dominates. Such a climatic trend could not be observed at the global scale because too many parameters vary contiguously and may hide specific trends.

The properties of sedimentary rocks contrast sharply with those of igneous rocks. They are easily eroded (high denudation rates and erodibility on Fig. 6) and obviously not as affected by threshold-controlled processes (low n for sedimentary rocks), being weaker (e.g., Sklar and Dietrich, 2001b;

Stock et al., 2005). These observations are enforced by the multiple regression analysis, where m/n, n, and K_{ref} for sedimentary rocks are obviously insensitive to seismicity, temperature, and precipitation, the forces behind most weathering processes. Metamorphic and mixed rock populations are more difficult to interpret based on our data set analysis.

3.4. Influence of tectonics

Figures 5 and 6 confirm previously published results. Namely, tectonically active areas generate more sediments (high denudation rates) and are the source locations of threshold-controlled, nonlinear processes (high n) compared to inactive areas (Molnar et al., 2007; Portenga and Bierman, 2011). We also find that erodibility seems to be reduced in active areas (Fig. 6). We are not sure how to explain this counterintuitive observation. The mean and median of K_{ref} may easily be influenced by third parameters such as MAP or vegetation. Figure 1 in the supplemental materials shows indeed a surprisingly clear population segmentation between tectonically active and inactive landscapes for vegetation. This may be explained by the correlation between elevation and other environmental parameters such as MAP, MAT, and vegetation. Active areas are indeed characterized by high elevation and exposed bedrock, therefore vegetation in active settings is expected to be scarce (Milodowski et al., 2015).

4. Potential limitations

Despite our best efforts to compile the finest global data set of cosmogenic denudation rates, many limitations and biases inherent to the actual

measurements remain and may alter the results detailed in the previous section. First, as shown in Fig. 2, the data are not distributed randomly. Large portions of the globe remain unexplored, while other areas (Himalayas, USA, Europe) concentrate most of the samples. This preferential sampling has a strong influence on the latitude variable, as areas between 20° and 50° north are overrepresented.

Secondly, sampling strategies vary between publications. Some authors specifically selected nested basins (covering a wide range of basin areas), while others concentrated their efforts on channel heads. These different approaches, coupled with the varying number of samples in each study, lead to important serial correlations. Large data sets are desirable for statistical purposes, but they introduce scale-dependent correlations. For instance, in Table 1, the sedimentary subcategory counts 63 samples. The analysis shows that more than 99% of the variability in K is accounted for in this subcategory(Table 1). The quality of this prediction is a consequence of the restricted repartition of the samples (only three areas). On the other hand, metamorphic zones are better sampled (eight zones), and as a consequence the explained variability for K drops to $< 60\%$ (with more than twice the number of samples).

Finally, ^{10}Be measurements can only be performed on quartz-rich rocks and sediments, thus considerably limiting the lithologies present in the data set (not all rocks contain quartz). Measuring ^{10}Be in other minerals (Nishiizumi et al., 1990) or using other isotopes altogether (Kober et al., 2009) may expand the scope of future studies. In that case, difficulties may arise from the cross calibrations between different isotope systems. We should also

point out that the stream power law (Eq. 1) gives a predictive relationship for erosion rates and not denudation rates as measured by cosmogenic data. Although chemical weathering processes are usually assumed to be negligible compared to physical processes, this assumption may be too strong for specific areas.

The presence of samples from glaciated or previously glaciated areas (as reported in the original publications) in our data set may induce an overestimation of the denudation rates and therefore affect the stream power law parameters estimation. About 40% of the subset samples come from areas that are or may have been glaciated in the past, although snow and ice shielding corrections, when available, have been included in the method to calculate the denudation rates. It is generally acknowledged that the influence of snow and the eventual presence of active/late Pleistocene glaciers on the calculation of denudation rates from cosmogenic nuclides is well within the error of the measure (about 10-15% reduction in the production rate; Wittmann et al. (2007); Scherler et al. (2014)). However, glacial and periglacial weathering processes may still have a strong effect on the observed denudation rates. For this reason and mostly for the fact that the stream power law is not suited to the study of landscapes carrying a glacial signal, such samples would ideally be omitted in future compilations.

Only about 3% of the sampled basins have an area below 5 km^2 (these 45 samples actually have an area ranging between 0.7 and 1 km^2). The influence of debris flows on the applicability of the stream power law should therefore be limited. To these potential issues, we need to add all the assumptions and uncertainties associated with the environmental global maps (MAP, MAT,

tree cover) and the cosmogenic measurement methods (uniform lithology, homogeneous mixing of the sediments, other sources of shielding, etc).

As explained in section 2.3, our method does not involve any assumptions on the steady-state/transience of the landscape. However, estimating a single M_χ value for a catchment may be problematic if the area is not at equilibrium. Segmented profiles may indeed display different slopes in χ-space, which can be attributed to spatial variations in lithology, uplift, or the propagation of transient signals through the landscape (Willenbring et al., 2013b).

It is a well known fact that correlations observed at the local scale often disappear, or are weaker, at the global scale (Portenga and Bierman, 2011). The influence of spatial scale on our results cannot be understated. Complex relationships between cause and effect operate from small scales to large scales as well as the reverse, and important large-scale features may appear without any preexisting heterogeneity at smaller scales, sometimes referred to as the concept of emergence (Murray et al., 2014). Therefore, caution should be applied when using small-scale measurements to interpret large-scale, complex systems such as climate. This complexity may be behind some of the unexpected results that came out of our analysis, for instance the lack of obvious correlation between erodibility and the mean annual precipitation.

A first step to improve the analysis of such an extensive data set would be to decorrelate interacting variables, in the manner of D'Arcy and Whittaker (2014) with orogenic precipitation. Indeed, an interpretation of climate subgroups remains weak as long as lithology or tectonic settings covary within

these groups. Ideally, for our purposes, subcategories should only have one fluctuating variable, all else being equal/uniform. For instance, within the cold climate subset, we should further subset the data to only retain zones of similar lithologies and tectonic activity, while making sure that these samples cover a wide range of locations across the globe (to prevent serial or dependent correlations). Unfortunately, such a rigorous approach remains largely unrealistic considering the lack of data. For our present data set, if we applied this strategy to the largest subgroups, we would only have 68 samples and four zones left to analyze (temperate climate, metamorphic rocks, and inactive tectonics), where MAT, MAP, and vegetation may still vary considerably.

5. Conclusion

We compile and recalculate worldwide basin-averaged denudation rates from previously published ^{10}Be concentrations. A unique global data set including more than 1450 samples, grouped into 59 zones, is analyzed to assess the stream power law parameters, namely the m/n ratio (or concavity index), the slope exponent n, and the erodibility coefficient K, using the integral method of channel profile analysis. These three parameters are quantified, largely for the first time, and form a compelling global scale experiment that can be explored to identify potential relationships with climate, lithology, and tectonics.

At the global scale, we find median values equal to 0.51 ± 0.14 for the concavity index, 2.43 ± 0.15 for the slope exponent and $2.9{*}10^{-10} \pm 1.0{*}10^{-9}$ for the normalized erodibility coefficient (using a reference concavity index

$m/n_{ref} = 0.5$). These values fall within the ranges predicted by theory and local field studies. The main feature is that the slope exponent is predominantly > 1, meaning that the relationship between denudation rate and the channel gradient is nonlinear. This result supports the idea that incision is a threshold controlled process. Recent publications back up the $n > 1$ estimate (DiBiase and Whipple, 2011; Whittaker and Boulton, 2012; Lague, 2014). Overall, our investigation fundamentally questions the application of the stream power model and the validity of many regional interpretations of climate and/or tectonics where the unity of n is routinely assumed. These studies may not reflect the actual behavior of channel bedrock erosion.

Furthermore, a multiple regression analysis demonstrates that intuitive or previously demonstrated local-scale trends, such as the correlation between K_{ref} and precipitation rates, do not appear at a global scale. The mean annual temperature and seismicity are the strongest regressors for n and K_{ref}, and mean annual precipitation is surprisingly the weakest. Overall, clear climatic trends could not be isolated from our analysis, although they may be present. The only reliable correlations appear for arid zones, featuring low n and high K_{ref} values, and igneous rocks (opposite trends). These results are intuitive and may be explained by various processes described in the literature.

Our results suggest that data from many sites are too sparse to predict n and K with a satisfying level of confidence. Indeed, based on the quality of the estimation, only 33 zones out of 59 (about 84% of the total samples) were used in our analysis ($\bar{p} \leq 0.16$ subset). However, a positive correlation between denudation rates and mean steepness index do appear for both the

global and the $\bar{p} \leq 0.16$ subset data. Several biases and gaps are pointed out in the existing data set, providing guidance for future data collection and analysis. Strategies to decorrelate or account for the complex interactions between incision processes, climate, and tectonics are especially desirable.

Acknowledgments

This work was supported by U.S. Army Research Office contract number W911NF-13-1-0478. The authors would like to thank Nicole M. Gasparini and an anonymous reviewer for their constructive and insightful comments. *Author Contributions* MAH and SMM wrote the analysis software. MAH performed the analysis. MAH wrote the paper with contributions from SMM and MA.

References

Andersen, J. L., Egholm, D. L., Knudsen, M. F., Jansen, J. D., Nielsen, S. B., Oct. 2015. The periglacial engine of mountain erosion - Part 1: Rates of frost cracking and frost creep. Earth Surface Dynamics 3 (4), 447–462.

Anderson, R. S., 1998. Near-Surface Thermal Profiles in Alpine Bedrock: Implications for the Frost Weathering of Rock. Arctic and Alpine Research 30 (4), 362–372.

Attal, M., Tucker, G. E., Whittaker, A. C., Cowie, P. A., Roberts, G. P., Sep. 2008. Modeling fluvial incision and transient landscape evolution: Influence of dynamic channel adjustment. Journal of Geophysical Research: Earth Surface 113 (F3), F03013.

Aubert, G., Langlois, V. J., Allemand, P., Apr. 2016. Bedrock incision by

bedload: insights from direct numerical simulations. Earth Surface Dynamics 4 (2), 327–342.

Balco, G., Stone, J. O., Lifton, N. A., Dunai, T. J., Aug. 2008. A complete and easily accessible means of calculating surface exposure ages or erosion rates from 10be and 26al measurements. Quaternary Geochronology 3 (3), 174–195.

Beer, A. R., Turowski, J. M., Jul. 2015. Bedload transport controls bedrock erosion under sediment-starved conditions. Earth Surface Dynamics 3 (3), 291–309.

Berner, R. A., Lasaga, A. C., Garrels, R. M., 1983. The carbonate-silicate geochemical cycle and its effect on atmospheric carbon dioxide over the past 100 million years. Am. J. Sci 283 (7), 641–683.

Bierman, P., Steig, E. J., 1996. Estimating rates of denudation using cosmogenic isotope abundances in sediment. Earth surface processes and landforms 21 (2), 125–139.

Bishop, P., 2007. Long-term landscape evolution: linking tectonics and surface processes. Earth Surface Processes and Landforms 32 (3), 329–365.

Braucher, R., Merchel, S., Borgomano, J., Bourls, D. L., Sep. 2011. Production of cosmogenic radionuclides at great depth: A multi element approach. Earth and Planetary Science Letters 309 (12), 1–9.

Chmeleff, J., von Blanckenburg, F., Kossert, K., Jakob, D., Jan. 2010. Determination of the 10be half-life by multicollector ICP-MS and liquid scin-

tillation counting. Nuclear Instruments and Methods in Physics Research Section B: Beam Interactions with Materials and Atoms 268 (2), 192–199.

Codilean, A. T., May 2006. Calculation of the cosmogenic nuclide production topographic shielding scaling factor for large areas using DEMs. Earth Surface Processes and Landforms 31, 785–794.

Collins, D. B. G., Bras, R., Tucker, G., 2004. Modeling the effects of vegetation-erosion coupling on landscape evolution. Journal of Geophysical Research: Earth Surface (2003–2012) 109 (F3).

Compo, G. P., Whitaker, J. S., Sardeshmukh, P. D., Matsui, N., Allan, R. J., Yin, X., Gleason, B. E., Vose, R. S., Rutledge, G., Bessemoulin, P., Brnnimann, S., Brunet, M., Crouthamel, R. I., Grant, A. N., Groisman, P. Y., Jones, P. D., Kruk, M. C., Kruger, A. C., Marshall, G. J., Maugeri, M., Mok, H. Y., Nordli, ., Ross, T. F., Trigo, R. M., Wang, X. L., Woodruff, S. D., Worley, S. J., Jan. 2011. The Twentieth Century Reanalysis Project. Quarterly Journal of the Royal Meteorological Society 137 (654), 1–28.

Coppus, R., Imeson, A., 2002. Extreme events controlling erosion and sediment transport in a semi-arid sub-andean valley. Earth Surface Processes and Landforms 27 (13), 1365–1375.

Cyr, A. J., Granger, D. E., Olivetti, V., Molin, P., 2014. Distinguishing between tectonic and lithologic controls on bedrock channel longitudinal profiles using cosmogenic 10 be erosion rates and channel steepness index. Geomorphology 209, 27–38.

D'Arcy, M., Whittaker, A. C., 2014. Geomorphic constraints on landscape sensitivity to climate in tectonically active areas. Geomorphology 204, 366–381.

DeFries, R., Hansen, M., Townshend, J., Janetos, A., Loveland, T., 2000. A new global 1-km dataset of percentage tree cover derived from remote sensing. Global Change Biology 6 (2), 247–254.

Delunel, R., Van Der Beek, P. A., Carcaillet, J., Bourlès, D. L., Valla, P. G., 2010. Frost-cracking control on catchment denudation rates: Insights from in situ produced 10 be concentrations in stream sediments (ecrins–pelvoux massif, french western alps). Earth and Planetary Science Letters 293 (1), 72–83.

Desilets, D., Zreda, M., Jan. 2003. Spatial and temporal distribution of secondary cosmic-ray nucleon intensities and applications to in situ cosmogenic dating. Earth and Planetary Science Letters 206 (12), 21–42.

DiBiase, R. A., Whipple, K. X., 2011. The influence of erosion thresholds and runoff variability on the relationships among topography, climate, and erosion rate. Journal of Geophysical Research: Earth Surface (2003–2012) 116 (F4).

DiBiase, R. A., Whipple, K. X., Heimsath, A. M., Ouimet, W. B., 2010. Landscape form and millennial erosion rates in the san gabriel mountains, ca. Earth and Planetary Science Letters 289 (1), 134–144.

Dunai, T. J., 2000. Scaling factors for production rates of in situ produced

cosmogenic nuclides: a critical reevaluation. Earth and Planetary Science Letters 176 (1), 157–169.

Dunne, J., Elmore, D., Muzikar, P., 1999. Scaling factors for the rates of production of cosmogenic nuclides for geometric shielding and attenuation at depth on sloped surfaces. Geomorphology 27 (1), 3–11.

Eppes, M. C., McFadden, L. D., Wegmann, K. W., Scuderi, L. A., Nov. 2010. Cracks in desert pavement rocks: Further insights into mechanical weathering by directional insolation. Geomorphology 123 (12), 97–108.

Ferrier, K. L., Huppert, K. L., Perron, J. T., 2013. Climatic control of bedrock river incision. Nature 496 (7444), 206–209.

Fielding, E., Isacks, B., Barazangi, M., Duncan, C., 1994. How flat is tibet? Geology 22 (2), 163–167.

Finnegan, N. J., Roe, G., Montgomery, D. R., Hallet, B., Mar. 2005. Controls on the channel width of rivers: Implications for modeling fluvial incision of bedrock. Geology 33 (3), 229–232.

Flint, J., 1974. Stream gradient as a function of order, magnitude, and discharge. Water Resources Research 10 (5), 969–973.

Gasparini, N. M., Brandon, M. T., Jun. 2011. A generalized power law approximation for fluvial incision of bedrock channels. Journal of Geophysical Research: Earth Surface 116 (F2), F02020.

Giardini, D., Grünthal, G., Shedlock, K. M., Zhang, P., 1999. The gshap global seismic hazard map. Annals of Geophysics 42 (6).

Godard, V., Burbank, D., Bourlès, D., Bookhagen, B., Braucher, R., Fisher, G., 2012. Impact of glacial erosion on 10be concentrations in fluvial sediments of the marsyandi catchment, central nepal. Journal of Geophysical Research: Earth Surface (2003–2012) 117 (F3).

Granger, D. E., Smith, A. L., Oct. 2000. Dating buried sediments using radioactive decay and muogenic production of 26al and 10be. Nuclear Instruments and Methods in Physics Research Section B: Beam Interactions with Materials and Atoms 172 (14), 822–826.

Hack, J. T., 1957. Studies of longitudinal stream profiles in virginia and maryland. Tech. rep.

Hales, T., Roering, J. J., 2007. Climatic controls on frost cracking and implications for the evolution of bedrock landscapes. Journal of Geophysical Research: Earth Surface (2003–2012) 112 (F2).

Heisinger, B., Lal, D., Jull, A., Kubik, P., Ivy-Ochs, S., Knie, K., Nolte, E., 2002a. Production of selected cosmogenic radionuclides by muons: 2. capture of negative muons. Earth and Planetary Science Letters 200 (3), 357–369.

Heisinger, B., Lal, D., Jull, A., Kubik, P., Ivy-Ochs, S., Neumaier, S., Knie, K., Lazarev, V., Nolte, E., 2002b. Production of selected cosmogenic radionuclides by muons: 1. fast muons. Earth and Planetary Science Letters 200 (3), 345–355.

Herman, F., Seward, D., Valla, P. G., Carter, A., Kohn, B., Willett, S. D.,

Ehlers, T. A., 2013. Worldwide acceleration of mountain erosion under a cooling climate. Nature 504 (7480), 423–426.

Hijmans, R. J., Cameron, S. E., Parra, J. L., Jones, P. G., Jarvis, A., et al., 2005. Very high resolution interpolated climate surfaces for global land areas. International journal of climatology 25 (15), 1965–1978.

Hobley, D. E. J., Sinclair, H. D., Mudd, S. M., Cowie, P. A., Dec. 2011. Field calibration of sediment flux dependent river incision. Journal of Geophysical Research: Earth Surface 116 (F4), F04017.

Howard, A. D., Kerby, G., 1983. Channel changes in badlands. Geological Society of America Bulletin 94 (6), 739–752.

Kirby, E., Whipple, K., 2001. Quantifying differential rock-uplift rates via stream profile analysis. Geology 29 (5), 415–418.

Kirby, E., Whipple, K. X., 2012. Expression of active tectonics in erosional landscapes. Journal of Structural Geology 44, 54–75.

Kober, F., Ivy-Ochs, S., Zeilinger, G., Schlunegger, F., Kubik, P., Baur, H., Wieler, R., 2009. Complex multiple cosmogenic nuclide concentration and histories in the arid rio lluta catchment, northern chile. Earth Surface Processes and Landforms 34 (3), 398–412.

Korschinek, G., Bergmaier, A., Faestermann, T., Gerstmann, U. C., Knie, K., Rugel, G., Wallner, A., Dillmann, I., Dollinger, G., von Gostomski, C. L., Kossert, K., Maiti, M., Poutivtsev, M., Remmert, A., Jan. 2010. A new value for the half-life of 10be by Heavy-Ion Elastic Recoil Detection and

liquid scintillation counting. Nuclear Instruments and Methods in Physics Research Section B: Beam Interactions with Materials and Atoms 268 (2), 187–191.

Lague, D., 2014. The stream power river incision model: evidence, theory and beyond. Earth Surface Processes and Landforms 39 (1), 38–61.

Lague, D., Hovius, N., Davy, P., 2005. Discharge, discharge variability, and the bedrock channel profile. Journal of Geophysical Research: Earth Surface (2003–2012) 110 (F4).

Lal, D., 1991. Cosmic ray labeling of erosion surfaces: in situ nuclide production rates and erosion models. Earth and Planetary Science Letters 104 (2-4), 424–439.

Lifton, N. A., Bieber, J. W., Clem, J. M., Duldig, M. L., Evenson, P., Humble, J. E., Pyle, R., 2005. Addressing solar modulation and long-term uncertainties in scaling secondary cosmic rays for in situ cosmogenic nuclide applications. Earth and Planetary Science Letters 239 (1), 140–161.

Meyer, H., Hetzel, R., Strauss, H., 2010. Erosion rates on different timescales derived from cosmogenic 10be and river loads: implications for landscape evolution in the rhenish massif, germany. International Journal of Earth Sciences 99 (2), 395–412.

Milodowski, D. T., Mudd, S. M., Mitchard, E. T., 2015. Erosion rates as a potential bottom-up control of forest structural characteristics in the sierra nevada mountains. Ecology 96 (1), 31–38.

Molnar, P., Anderson, R. S., Anderson, S. P., 2007. Tectonics, fracturing of rock, and erosion. Journal of Geophysical Research: Earth Surface (2003–2012) 112 (F3).

Mudd, S. M., Attal, M., Milodowski, D. T., Grieve, S. W., Valters, D. A., 2014. A statistical framework to quantify spatial variation in channel gradients using the integral method of channel profile analysis. Journal of Geophysical Research: Earth Surface 119 (2), 138–152.

Murray, A. B., Coco, G., Goldstein, E. B., 2014. Cause and effect in geomorphic systems: Complex systems perspectives. Geomorphology 214, 1–9.

Nishiizumi, K., Imamura, M., Caffee, M. W., Southon, J. R., Finkel, R. C., McAninch, J., May 2007. Absolute calibration of 10be AMS standards. Nuclear Instruments and Methods in Physics Research Section B: Beam Interactions with Materials and Atoms 258 (2), 403–413.

Nishiizumi, K., Klein, J., Middleton, R., Craig, H., 1990. Cosmogenic 10 be, 26 al, and 3 he in olivine from maui lavas. Earth and Planetary Science Letters 98 (3), 263–266.

Norton, K. P., Vanacker, V., 2009. Effects of terrain smoothing on topographic shielding correction factors for cosmogenic nuclide-derived estimates of basin-averaged denudation rates. Earth Surface Processes and Landforms 34 (1), 145–154.

Norton, K. P., von Blanckenburg, F., Schlunegger, F., Schwab, M., Kubik, P. W., 2008. Cosmogenic nuclide-based investigation of spatial erosion and

hillslope channel coupling in the transient foreland of the swiss alps. Geomorphology 95 (3), 474–486.

Peel, M. C., Finlayson, B. L., McMahon, T. A., 2007. Updated world map of the köppen-geiger climate classification. Hydrology and Earth System Sciences Discussions Discussions 4 (2), 439–473.

Perron, J. T., Royden, L., 2013. An integral approach to bedrock river profile analysis. Earth Surface Processes and Landforms 38 (6), 570–576.

Portenga, E. W., Bierman, P. R., 2011. Understanding earths eroding surface with 10 be. GSA Today 21 (8), 4–10.

Riebe, C. S., Kirchner, J. W., Granger, D. E., Finkel, R. C., 2001a. Minimal climatic control on erosion rates in the sierra nevada, california. Geology 29 (5), 447–450.

Riebe, C. S., Kirchner, J. W., Granger, D. E., Finkel, R. C., 2001b. Strong tectonic and weak climatic control of long-term chemical weathering rates. Geology 29 (6), 511–514.

Royden, L., Clark, M., Whipple, K., 2000. Evolution of river elevation profiles by bedrock incision: Analytical solutions for transient river profiles related to changing uplift and precipitation rates. Eos Trans. AGU 81, 48.

Royden, L., Perron, J., Jun. 2013. Solutions of the stream power equation and application to the evolution of river longitudinal profiles. Journal of Geophysical Research: Earth Surface 118 (2), 497–518.

Scherler, D., Bookhagen, B., Strecker, M. R., 2014. Tectonic control on 10be-derived erosion rates in the garhwal himalaya, india. Journal of Geophysical Research: Earth Surface 119 (2), 83–105.

Sklar, L. S., Dietrich, W. E., Dec. 2001a. Sediment and rock strength controls on river incision into bedrock. Geology 29 (12), 1087–1090.

Sklar, L. S., Dietrich, W. E., 2001b. Sediment and rock strength controls on river incision into bedrock. Geology 29 (12), 1087–1090.

Slater, L. J., Singer, M. B., 2013. Imprint of climate and climate change in alluvial riverbeds: Continental united states, 1950-2011. Geology 41 (5), 595–598.

Slingerland, R., Willett, S., Hovius, N., 1998. Slope-area scaling as a test of fluvial bedrock erosion laws. Eos Trans. AGU 79, 45.

Smith, B. J., Warke, P. A., McGreevy, J. P., Kane, H. L., Apr. 2005. Salt-weathering simulations under hot desert conditions: agents of enlightenment or perpetuators of preconceptions? Geomorphology 67 (12), 211–227.

Stock, J., Dietrich, W. E., 2003. Valley incision by debris flows: Evidence of a topographic signature. Water Resources Research 39 (4).

Stock, J. D., Montgomery, D. R., 1999. Geologic constraints on bedrock river incision using the stream power law. Journal of Geophysical Research: Solid Earth (1978–2012) 104 (B3), 4983–4993.

Stock, J. D., Montgomery, D. R., Collins, B. D., Dietrich, W. E., Sklar, L., 2005. Field measurements of incision rates following bedrock exposure:

Implications for process controls on the long profiles of valleys cut by rivers and debris flows. Geological Society of America Bulletin 117 (1-2), 174–194.

Stone, J. O., Oct. 2000. Air pressure and cosmogenic isotope production. Journal of Geophysical Research 105, 23753.

Thiede, R. C., Ehlers, T. A., 2013. Large spatial and temporal variations in himalayan denudation. Earth and Planetary Science Letters 371, 278–293.

Tucker, G., Whipple, K., 2002. Topographic outcomes predicted by stream erosion models: Sensitivity analysis and intermodel comparison. Journal of Geophysical Research: Solid Earth 107 (B9).

Tucker, G. E., McCoy, S. W., Whittaker, A. C., Roberts, G. P., Lancaster, S. T., Phillips, R., 2011. Geomorphic significance of postglacial bedrock scarps on normal-fault footwalls. Journal of Geophysical Research: Earth Surface (2003–2012) 116 (F1).

Turowski, J. M., Lague, D., Hovius, N., Dec. 2007. Cover effect in bedrock abrasion: A new derivation and its implications for the modeling of bedrock channel morphology. Journal of Geophysical Research: Earth Surface 112 (F4), F04006.

Vermeesch, P., 2007. CosmoCalc: An Excel add-in for cosmogenic nuclide calculations. Geochemistry, Geophysics, Geosystems 8 (8), Q08003.

Von Blanckenburg, F., 2005. The control mechanisms of erosion and weathering at basin scale from cosmogenic nuclides in river sediment. Earth and Planetary Science Letters 237 (3), 462–479.

Walder, J., Hallet, B., Mar. 1985. A theoretical model of the fracture of rock during freezing. Geological Society of America Bulletin 96 (3), 336–346.

Whipple, K. X., 2004. Bedrock rivers and the geomorphology of active orogens. Annu. Rev. Earth Planet. Sci. 32, 151–185.

Whipple, K. X., Hancock, G. S., Anderson, R. S., 2000. River incision into bedrock: Mechanics and relative efficacy of plucking, abrasion, and cavitation. Geological Society of America Bulletin 112 (3), 490–503.

Whipple, K. X., Tucker, G. E., 1999. Dynamics of the stream-power river incision model: Implications for height limits of mountain ranges, landscape response timescales, and research needs. Journal of Geophysical Research: Solid Earth (1978–2012) 104 (B8), 17661–17674.

Whittaker, A. C., Boulton, S. J., 2012. Tectonic and climatic controls on knickpoint retreat rates and landscape response times. Journal of Geophysical Research: Earth Surface (2003–2012) 117 (F2).

Whittaker, A. C., Cowie, P. A., Attal, M., Tucker, G. E., Roberts, G. P., Feb. 2007. Bedrock channel adjustment to tectonic forcing: Implications for predicting river incision rates. Geology 35 (2), 103–106.

Willenbring, J. K., Codilean, A. T., McElroy, B., 2013a. Earth is (mostly) flat: Apportionment of the flux of continental sediment over millennial time scales. Geology 41 (3), 343–346.

Willenbring, J. K., Gasparini, N. M., Crosby, B. T., Brocard, G., 2013b. What does a mean mean? the temporal evolution of detrital cosmogenic denudation rates in a transient landscape. Geology 41 (12), 1215–1218.

Wittmann, H., von Blanckenburg, F., Kruesmann, T., Norton, K. P., Kubik, P. W., 2007. Relation between rock uplift and denudation from cosmogenic nuclides in river sediment in the central alps of switzerland. Journal of Geophysical Research: Earth Surface (2003–2012) 112 (F4).

Wobus, C., Whipple, K. X., Kirby, E., Snyder, N., Johnson, J., Spyropolou, K., Crosby, B., Sheehan, D., 2006. Tectonics from topography: Procedures, promise, and pitfalls. Geological Society of America Special Papers 398, 55–74.

Wolman, M. G., Gerson, R., 1978. Relative scales of time and effectiveness of climate in watershed geomorphology. Earth surface processes 3 (2), 189–208.